

# NUMERICAL SOLUTIONS OF A VECTOR GINZBURG-LANDAU EQUATION WITH A TRIPLE WELL POTENTIAL

John M. Neuberger, Dennis R. Rice, Jr. and James W. Swift

*Department of Mathematics and Statistics, Northern Arizona University, Box 5717, Flagstaff, AZ 86001*

## Abstract

We numerically compute solutions to the vector Ginzburg-Landau equation with a triple-well potential. We use the Galerkin Newton Gradient Algorithm of Neuberger & Swift and bifurcation techniques to find solutions. With a small parameter, we find a Morse index 2 triple junction solution. This is the solution for which Flores, Padilla, & Tonegawa gave an existence proof. We classify all of the solutions guaranteed to exist by the Equivariant Branching Lemma at the first bifurcation points of the trivial solutions. Guided by the symmetry analysis, we numerically compute the solution branches.

*Revised manuscript submitted to the International Journal of Bifurcation and Chaos on August 28, 2002*

## 1 Introduction

This paper is an extension of two other papers. We take a problem studied by Flores, Padilla & Tonegawa [2001] and use the algorithm developed by Neuberger & Swift [2001] to investigate it. Flores, Padilla & Tonegawa study a vector Ginzburg-Landau equation

$$\begin{cases} -\epsilon^2 \Delta u + \nabla W(u) = 0 & \text{in } \Omega \\ \frac{\partial u}{\partial \eta} = 0 & \text{on } \partial\Omega, \end{cases} \quad (1)$$

where  $\Omega \subset \mathbf{R}^2$  is a bounded regular domain,  $u : \Omega \rightarrow \mathbf{R}^2$ ,  $W : \mathbf{R}^2 \rightarrow [0, \infty)$  is a triple-well potential,  $\eta$  is the unit outer normal to the boundary, and  $\epsilon > 0$  is a parameter. The gradient in  $\nabla W(u)$  is with respect to  $u$ , hence  $\nabla W = (\partial W / \partial u_1, \partial W / \partial u_2)$ . We will work with sufficiently smooth functions  $u \in L^2 \times L^2$ , where  $L^2 = L^2(\Omega)$ . For simplicity, we consider the unit square  $\Omega = (0, 1) \times (0, 1)$ .

One of our initial objectives in this research was to demonstrate the utility of the so-called Gradient Newton Galerkin Algorithm (GNGA) from [Neuberger & Swift, 2001] in investigating *systems* of nonlinear elliptic PDE. Once we had successfully implemented the algorithm for systems, we looked for an interesting application to test it on, and found system (1). To quote [Flores, Padilla, & Tonegawa, 2002] directly (see the paper for references), “This problem appears in several physical contexts, including the study of motion of grain boundaries in alloys, capillary phenomena and certain models for phase transitions in the so-called mean-field approximation”. We are successful in numerically computing the triple junction configuration discussed in Flores, Padilla, & Tonegawa [2002]. We numerically captured features both proved and conjectured to exist. Additionally, we have classified the most symmetric types of solutions bifurcating from the trivial branches at the first bifurcation points. By this we mean that we numerically locate all branches that our bifurcation analysis suggests should exist, and do not observe any other branches. A computation of the error gives one confidence that the solutions we find are not spurious.

Much has been done in the area of numerical bifurcation analysis for nonlinear elliptic PDE (see for example [Mei, 2000], [Allgower & Georg, 1990], and references therein). In particular, a scalar equation with zero Dirichlet boundary condition is studied in [Allgower, Böhmer, & Zhen, 1994], where they also use symmetry to investigate a corank-4 bifurcation similar to the one we study in Section 3. While our algorithm and consequent implementation have proven to be sufficient for our needs, it is entirely likely that techniques known to these and other authors (see for example [Bank & Mittelmann, 1989]) would improve our numerical

performance. Our algorithm is distinct from other Galerkin type algorithms found in the literature. We do not use a basis of finite elements, rather a basis of eigenfunctions of the linear part of the problem.

Flores, Padilla & Tonegawa [2001] use the existence of three Morse index (MI) 1 mountain pass solutions to prove the existence of a MI 2 solution. When  $\epsilon$  is small, none of the trivial solutions have MI 2, so the solution they find must be nontrivial. In [Neuberger & Swift, 2001], we applied the GNGA to a single nonlinear elliptic PDE with zero Dirichlet boundary conditions. Here, we apply the algorithm to a system with zero Neumann boundary conditions. We use the techniques of symmetric bifurcation theory (see for example [Golubitsky, Stewart & Schaeffer, 1988] and [Sattinger, 1979]) to guide our numerical investigation. We approximate the nontrivial MI 2 solution proved to exist by Flores, Padilla & Tonegawa [2001], and confirm their conjecture that it has a triple junction.

The proofs of [Flores, Padilla & Tonegawa, 2001] involve study of the negative gradient flow associated with the variational elliptic system (1). The negative gradient flow is a parabolic system for  $\tilde{u} : \mathbf{R}^+ \times \Omega \rightarrow \mathbf{R}^2$ :

$$\tilde{u}_t = -\epsilon \nabla J_\epsilon(\tilde{u}) = \epsilon^2 \Delta \tilde{u} - \nabla W(\tilde{u}), \quad (2)$$

where the energy functional is defined by

$$J_\epsilon(u) = \frac{1}{\epsilon} \int_{\Omega} \left( \frac{\epsilon^2}{2} |\nabla u|^2 + W(u) \right) dx dy. \quad (3)$$

The solutions to elliptic system (1) are the steady state solutions of (2). Our definition of  $J_\epsilon$  agrees with Flores et al. They include the factor of  $1/\epsilon$  because solutions with finite  $J_\epsilon$  in the limit  $\epsilon \rightarrow 0$  play a special role in their analysis.

The Morse index of a nondegenerate critical point of a functional  $J$  is the number of negative eigenvalues of  $J''$ , evaluated at the critical point (see [Milnor, 1963]). In the context of the negative gradient flow, the Morse index of a critical point is the number of unstable eigenvalues of the linearized flow.

Following [Flores, Padilla & Tonegawa, 2001], we assume that the following conditions of  $W$  are satisfied:

- (i)  $W(u) \geq 0$  for all  $u \in \mathbf{R}^2$ .
- (ii)  $P_1 = a$ ,  $P_2 = b$  and  $P_3 = c \in \mathbf{R}^2$  are three different points such that  $W(a) = W(b) = W(c) = 0$ , i.e., global minima of  $W$ . We will also suppose that these points are nondegenerate. For simplicity we will take these as the only minima of the potential.
- (iii)  $W$  is uniformly coercive in  $u$ , that is, there exist  $R_0$  and  $C > 0$  such that if  $|u| \geq R_0$  then  $W(u) \geq C|u|^2$ . We assume that  $R_0$  was chosen sufficiently large so that the negative gradient flow of  $W$  points towards the ball  $B_{R_0}(0)$  at points outside the ball.

In our investigation we take  $\Omega = (0, 1) \times (0, 1)$  and

$$W(u_1, u_2) = \alpha - (u_1^2 + u_2^2) + \beta(u_1^2 + u_2^2)^2 - \gamma(u_1^3 - 3u_1u_2^2),$$

where  $\alpha$ ,  $\beta$ , and  $\gamma \in \mathbf{R}^+$ . The critical points of  $W$  that lie on the  $u_1$ -axis are the simplest to analyze. They satisfy a cubic equation that factors, and has the roots  $u_1 = 0, (3\gamma \pm \sqrt{32\beta + 9\gamma^2})/(8\beta)$ . We used the parameters  $\beta \approx 0.1312$  and  $\gamma \approx 0.1316$ , and define  $u_{\min}$ ,  $u_s$ , and  $u_{\max}$  to be the minimum, saddle and (local) maximum points of  $W$ , respectively, which lie on the  $u_1$  axis:

$$u_{\min} \approx (2.364, 0), \quad u_s \approx (-1.612, 0), \quad \text{and} \quad u_{\max} = (0, 0). \quad (4)$$

The other critical points follow from the symmetry of the potential, as seen in Figure 1. The value of  $\alpha$  was then chosen to make 0 the minimum value of  $W$ , giving the critical values:

$$W_{\min} := W(u_{\min}) = 0, \quad W_s := W(u_s) \approx 2.069, \quad \text{and} \quad W_{\max} := W(u_{\max}) \approx 3.230. \quad (5)$$

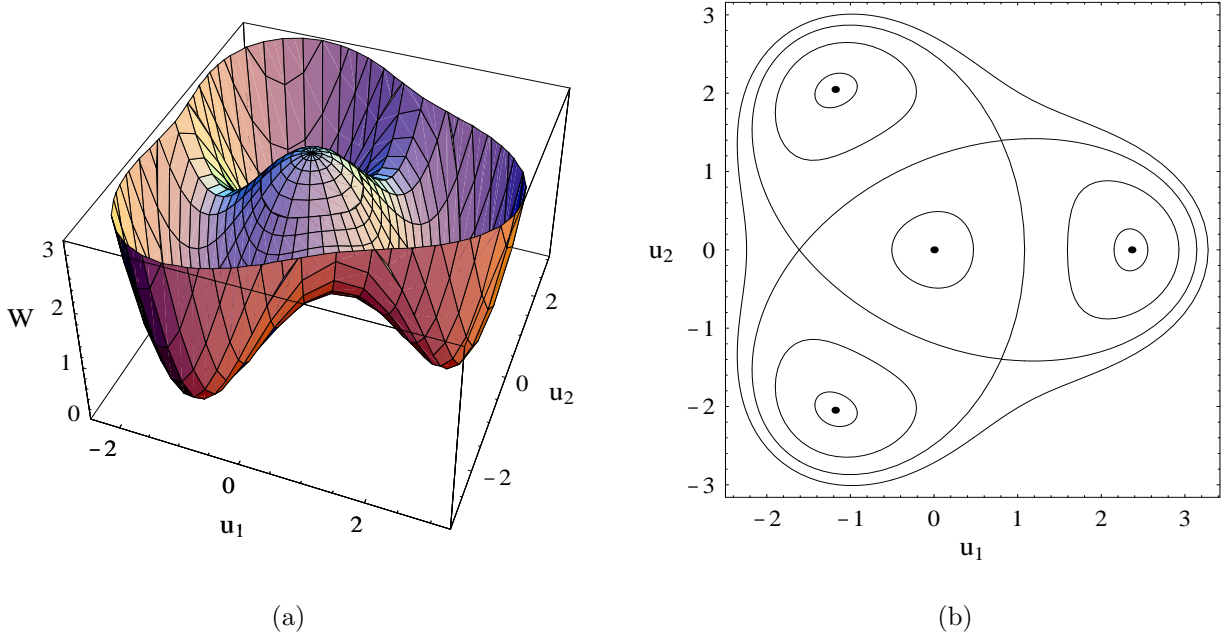


Figure 1: The triple-well potential  $W$ . Part (a) is the graph of  $W$ . Part (b) shows the minima and local maximum of  $W$  as dots, as well as the contours  $W(u_1, u_2) = 0.1, 1, W_s \approx 2.069$ , and 3.

## 2 Implementing GNGA

The eigenvalues and eigenfunctions of  $-\Delta$  on the unit square with zero Neumann boundary conditions are well known. The (doubly-indexed) eigenvalues of  $-\Delta$  are  $\lambda_{m,n} = (m^2 + n^2)\pi^2$  and the eigenfunctions  $\psi_{m,n}$  of  $-\Delta$ , normalized in  $L^2$ , are given by:

$$\psi_{m,n}(x, y) = \begin{cases} 1 & \text{for } m = n = 0 \\ \sqrt{2} \cos(m\pi x) \cos(n\pi y) & \text{for } m = 0, n \neq 0 \text{ or } n = 0, m \neq 0 \\ 2 \cos(m\pi x) \cos(n\pi y) & \text{for } m \neq 0 \text{ and } n \neq 0, \end{cases}$$

where  $m$  and  $n$  range over all of the nonnegative integers. It is well known that  $\{\psi_{m,n}\}$  forms a basis for  $L^2$  and  $H = H^{1,2}(\Omega)$  [Adams, 1975]. We obtain a finite sub-basis of  $L^2$  or  $H$  by choosing a positive integer  $k$ , and including all eigenfunctions whose eigenvalues are strictly less than  $\pi^2 k^2$ . These eigenvalues are then ordered and singly indexed as  $\lambda_1 = 0 < \lambda_2 \leq \lambda_3 \leq \dots \leq \lambda_{\tilde{M}}$ . This yields a singly indexed basis,  $\{\psi_i\}$ , of size  $\tilde{M}$ . In the current work,  $k$  is an even integer ranging from  $k = 8$  ( $\tilde{M} = 56$ ) up to  $k = 18$  ( $\tilde{M} = 269$ ). As a rule of thumb, we trust a numerical calculation if the results are not significantly changed when the cutoff parameter  $k$  is increased by 2.

We use the following Galerkin subspace of  $H \times H$  and  $L^2 \times L^2$ :

$$G = \text{Span} \left\{ \left( \begin{array}{c} \psi_i \\ 0 \end{array} \right) \right\}_{i=1}^{\tilde{M}} \cup \left\{ \left( \begin{array}{c} 0 \\ \psi_i \end{array} \right) \right\}_{i=1}^{\tilde{M}},$$

which is of dimension  $M = 2\tilde{M}$ . For convenience, we use  $\{\Psi_i\}_{i=1}^M$  to denote this basis. So, for  $u \in G$ , there exist unique Fourier coefficients  $a \in \mathbf{R}^M$  such that  $u = \sum_{i=1}^M a_i \Psi_i$ .

As previously stated, GNGA uses a variational method to solve (1). The energy functional  $J_\epsilon : H \times H \rightarrow \mathbf{R}$  is defined in equation (3). For convenience we sometimes write  $J$  for  $J_\epsilon$ . It is well known that critical points

of  $J$  are exactly the classical solutions to (1) (see [Gilbarg & Trudinger, 1983]). To apply GNGA, we need to compute first and second directional derivatives of  $J$ . A calculation shows that the directional derivative of  $J$  at  $u$  in the  $\Psi_j$  direction is

$$\begin{aligned} g_j(u) := J'(u)(\Psi_j) &= \int_{\Omega} \left( \epsilon \nabla u \cdot \nabla \Psi_j + \frac{1}{\epsilon} \Psi_j \cdot \nabla W(u) \right) dx dy \\ &= \int_{\Omega} \left( \epsilon \sum_{i=1}^M a_i (\nabla \Psi_i \cdot \nabla \Psi_j) + \frac{1}{\epsilon} \Psi_j \cdot \nabla W(u) \right) dx dy \\ &= \epsilon a_j \lambda_j + \frac{1}{\epsilon} \int_{\Omega} \Psi_j \cdot \nabla W(u) dx dy. \end{aligned}$$

Similarly, the second directional derivative is computed to be

$$\begin{aligned} A_{jk}(u) := J''(u)(\Psi_j, \Psi_k) &= \int_{\Omega} \left( \epsilon \nabla \Psi_j \cdot \nabla \Psi_k + \frac{1}{\epsilon} D^2 W(u) \Psi_j \cdot \Psi_k \right) dx dy \\ &= \epsilon \lambda_j \delta_{jk} + \frac{1}{\epsilon} \int_{\Omega} D^2 W(u) \Psi_j \cdot \Psi_k dx dy, \end{aligned}$$

where  $\delta_{jk}$  is the Kronecker delta function. The algorithm, GNGA, consists of performing Newton's method iterations on the Fourier coefficients to find zeros of  $g$ .

The  $L^2$  Hessian and gradient are only densely defined [Neuberger, 1997]. Where defined,

$$\begin{aligned} J'(u)(v) &= \langle \nabla J(u), v \rangle_2 \text{ and} \\ J''(u)(v, w) &= \langle D^2 J(u)v, w \rangle_2. \end{aligned}$$

The quantities  $\nabla J(u)$  and  $D^2 J(u)$  are defined on all of  $G$ . Furthermore, the Sobolev gradient,  $\nabla_H J(u)$ , and the Hessian,  $D_H^2 J(u)$ , satisfy

$$(D_H^2 J(u))^{-1} \nabla_H J(u) = (D^2 J(u))^{-1} \nabla J(u)$$

for all  $u \in G$ . Hence, we may use the  $L^2$  gradient and Hessian in our implementation of the Newton algorithm, (see [Neuberger & Swift, 2001] and [Neuberger, 1997] for more details). We use Fourier coefficients of the term  $(D^2 J(u))^{-1} \nabla J(u)$  as the search direction in our algorithm. In our algorithm, the  $M \times M$  matrix  $A$  represents  $D^2 J(u)$ , the elements of the vector  $g \in \mathbf{R}^M$  are the Fourier coefficients of  $P_G \nabla J(u)$ , and the vector  $\chi \in \mathbf{R}^M$  is the search direction given by  $A\chi = g$ . Since the  $L^2$  Hessian is not always invertible, we use a least-squares solver to compute this search direction. Alternatively, one could use a pseudo-inverse or, if the Hessian is known to be invertible, one could solve the equation directly. Also it is of use to us to compute the number of negative eigenvalues of  $A$ , denoted  $\text{sig}(A)$ . Note that  $\text{sig}(A)$  corresponds to the MI of  $u$  provided that  $u$  is a nondegenerate critical point of  $J$  and  $M$  is sufficiently large.

### The Algorithm

- Choose initial coefficients  $a = a^0 = \{a_k\}_{k=1}^M$ , set  $u = u^0 = \sum a_k \Psi_k$ , choose a tolerance  $TOL$ , choose  $\delta$  equal to the desired Newton step size, and set the loop counter  $n = 0$ .
- Loop:
  1. Calculate  $g = g^{n+1} = (J'(u)(\Psi_k))_{k=1}^M \in \mathbf{R}^M$  (gradient vector).
  2. Calculate  $A = A^{n+1} = (J''(u)(\Psi_j, \Psi_k))_{j,k=1}^M$  (Hessian matrix).
  3. Compute  $\chi = \chi^{n+1} = A^{-1}g$  using a least-squares solver to solve  $A\chi = g$  (search direction).
  4. Set  $a = a^{n+1} = a^n - \delta\chi$  and update  $u = u^{n+1} = \sum_{k=1}^M a_k \Psi_k$ .
  5. Increment loop counter.
  6. Calculate the Morse index of  $u$  (i.e.,  $\text{sig}(A)$ ) and  $J(u)$ .
  7. Calculate  $\sqrt{g \cdot g} = \|P_G \nabla J(u)\|$ ; STOP if  $\sqrt{g \cdot g} < TOL$ .

### 3 Local Bifurcations of the Trivial Solutions

The triple-well potential,  $W$ , has exactly seven critical points: three global minima, three saddle points, and a local maximum. Each of these critical points corresponds to a trivial (constant) solution of (1). Because of the symmetry of the potential, we only need to consider the critical points of  $W$  on the  $u_1$ -axis, which are listed in equation (4). The three solutions of (1) corresponding to these critical points of  $W$  are called the minimum solution  $u \equiv u_{\min}$ , the saddle solution  $u \equiv u_s$ , and the maximum solution  $u \equiv u_{\max}$ .

In this section we linearize the system (1) about each of these trivial solutions, and study a few local bifurcations of these solutions. Our goal is to obtain bifurcation diagrams of  $J_\epsilon(u)$  versus  $\epsilon$  for the trivial solutions and the solutions which bifurcate from them at the “first” bifurcation.

The energy of each trivial solution depends on the corresponding critical value of the potential (5):

$$J_\epsilon(u_{\min}) = \frac{W_{\min}}{\epsilon} = 0, \quad J_\epsilon(u_s) = \frac{W_s}{\epsilon} \approx \frac{2.069}{\epsilon}, \quad \text{and} \quad J_\epsilon(u_{\max}) = \frac{W_{\max}}{\epsilon} \approx \frac{3.230}{\epsilon}.$$

The Hessian  $D^2J(u)$  is easy to analyze when  $u$  is a constant function,  $u \equiv u^*$ . When  $u^*$  is on the  $u_1$ -axis the eigenvalues and eigenfunctions of  $\epsilon D^2J(u^*)$  are

$$\begin{aligned} &\text{eigenvalue } \epsilon^2 \lambda_{m,n} + e_1(u^*) \quad \text{with eigenfunction } (\psi_{m,n}, 0) \text{ and} \\ &\text{eigenvalue } \epsilon^2 \lambda_{m,n} + e_2(u^*) \quad \text{with eigenfunction } (0, \psi_{m,n}). \end{aligned}$$

where  $e_1(u^*)$  and  $e_2(u^*)$  are the eigenvalues of  $D^2W(u^*)$  with eigenvectors  $(1, 0)$  and  $(0, 1)$ , respectively. Note that we have used the doubly indexed eigenvalues  $(\lambda_{m,n})$  and eigenfunctions  $(\psi_{m,n})$  of the negative Laplacian, defined at the beginning of section 2. For our choice of potential, the eigenvalues of  $D^2W$  evaluated at the critical points are

$$\begin{aligned} e_1(u_{\min}) &\approx 4.934 \text{ and } e_2(u_{\min}) \approx 2.801, \\ e_1(u_s) &\approx 3.363 \text{ and } e_2(u_s) \approx -1.910, \text{ and} \\ e_1(u_{\max}) &= e_2(u_{\max}) = -2. \end{aligned} \tag{6}$$

The Morse index of a solution is the number of negative eigenvalues of the Hessian  $D^2J(u)$ , assuming that none of the eigenvalues are zero. It is clear that the MI of  $u_{\min}$  is 0 for all  $\epsilon$ , since  $e_1(u_{\min})$  and  $e_2(u_{\min})$  are positive and  $\lambda_{m,n} \geq 0$ . The MI of  $u_s$  is the cardinality of the set  $\{(m, n) \in \mathbf{N}^2 \mid \epsilon^2 \lambda_{m,n} < -e_2(u_s) \approx 1.910\}$ , where  $\mathbf{N}$  is the set of nonnegative integers. Similarly, the MI of  $u_{\max}$  is twice the cardinality of the set  $\{(m, n) \in \mathbf{N}^2 \mid \epsilon^2 \lambda_{m,n} < 2\}$ .

Recall that  $\lambda_{0,0} = 0$ , and all other eigenvalues are strictly positive. Hence, when  $\epsilon$  is sufficiently large, the MI of the saddle solution is 1 and the MI of the maximum solution is 2. Furthermore, the set of eigenvalues  $\{\lambda_{m,n}\}$  has no upper bound, so the Morse indices of the trivial solutions  $u_s$  and  $u_{\max}$  increase without bound as  $\epsilon \rightarrow 0$ . We will now investigate the first bifurcation of the saddle and maximum solutions as  $\epsilon$  is decreased.

The first bifurcation of the saddle solution occurs at  $\epsilon = \sqrt{-e_2(u_s)}/\pi \approx 0.4399$ . The critical eigenspace is

$$\{u = u_s + (0, b_{10}\psi_{1,0} + b_{01}\psi_{0,1}) \mid (b_{01}, b_{10}) \in \mathbf{R}^2\}. \tag{7}$$

The first bifurcation of the maximum solution occurs at  $\epsilon = \sqrt{2}/\pi \approx 0.4502$ . The critical eigenspace is

$$\{u = (a_{10}\psi_{1,0} + a_{01}\psi_{0,1}, b_{10}\psi_{1,0} + b_{01}\psi_{0,1}) \mid (a_{01}, a_{10}, b_{01}, b_{10}) \in \mathbf{R}^4\}. \tag{8}$$

To follow a bifurcation branch numerically with the GNGA, we set  $\epsilon$  just below the bifurcation value, and make an initial guess in the critical eigenspace. After a solution is found,  $\epsilon$  is stepped down, using the solution found at the previous  $\epsilon$  as the initial guess. The success of this method requires a good guess near the bifurcation. With a two dimensional eigenspace it is not trivial to find an initial guess for which Newton’s method converges. The problem is even worse with a four dimensional eigenspace. It is easy to get lost in  $\mathbf{R}^4$  without a good map. The symmetry of the PDE (1) causes the critical eigenspaces to have dimension larger than one. On the other hand, the symmetry comes to the rescue through the Equivariant Branching Lemma (EBL, see [Vanderbauwhede, 1982] and [Golubitsky, Stewart & Schaeffer, 1986]), which provides the

“map” to tell us where to look for solutions near the bifurcation. The rest of this section describes how we use symmetric bifurcation theory (see [Golubitsky, Stewart & Schaeffer, 1986] and Sattinger [1979]) to predict where the small amplitude solutions lie within the critical eigenspaces.

Liapunov-Schmidt reduction can be used to find small amplitude solutions of the PDE (1) corresponding to solutions of a reduced system of equations  $f(x) = 0$ . At the bifurcation of the saddle solution,  $f : \mathbf{R}^2 \rightarrow \mathbf{R}^2$  and  $x = (b_{01}, b_{01}) \in \mathbf{R}^2$ . At the bifurcation of the maximum solution,  $f : \mathbf{R}^4 \rightarrow \mathbf{R}^4$  and  $x = (a_{01}, a_{01}, b_{01}, b_{01}) \in \mathbf{R}^4$ . Alternatively, the center manifold theorem can be used to give the ODE  $\dot{x} = f(x)$  whose solutions correspond to solutions of the negative gradient flow (2).

The reduced vector fields  $f$  are equivariant because they inherit symmetry from the original system (1). The equivariant branching lemma (see [Vanderbauwhede, 1982] and [Golubitsky, Stewart & Schaeffer, 1986]) states that certain solutions must bifurcate from the trivial solution, assuming nondegeneracy conditions hold. The solutions which bifurcate are one-dimensional fixed point subspaces of the action of the finite group on  $\mathbf{R}^n$ .

The symmetry of the system (1) is  $D_4 \times D_3$ , where  $D_n$  is the symmetry of a regular  $n$ -gon. A set of generators of the symmetry is listed in Table 1, along with the action of the generator on the critical eigenspace.

Symmetry of the PDE	Action on Eigenspace (7)	Action on Eigenspace (8)
$(x, y) \mapsto (1 - x, y)$	$(b_{10}, b_{01}) \mapsto (-b_{10}, b_{01})$	$(a_{10}, a_{01}, b_{10}, b_{01}) \mapsto (-a_{10}, a_{01}, -b_{10}, b_{01})$
$(x, y) \mapsto (y, x)$	$(b_{10}, b_{01}) \mapsto (b_{01}, b_{10})$	$(a_{10}, a_{01}, b_{10}, b_{01}) \mapsto (a_{01}, a_{10}, b_{01}, b_{10})$
$u_1 + iu_2 \mapsto e^{i2\pi/3}(u_1 + iu_2)$	Not Applicable	$\begin{cases} a_{10} + ib_{10} \mapsto e^{i2\pi/3}(a_{10} + ib_{10}) \\ a_{01} + ib_{01} \mapsto e^{i2\pi/3}(a_{01} + ib_{01}) \end{cases}$
$(u_1, u_2) \mapsto (u_1, -u_2)$	$(b_{10}, b_{01}) \mapsto (-b_{10}, -b_{01})$	$(a_{10}, a_{01}, b_{10}, b_{01}) \mapsto (a_{10}, a_{01}, -b_{10}, -b_{01})$

Table 1: Generators of the  $D_4 \times D_3$  symmetry, along with their action on the critical eigenspaces. The first two rows are generators of  $D_4$ , and the last two rows are generators of  $D_3$ . One entry is blank because the  $120^\circ$  rotation in the  $(u_1, u_2)$  plane does not map the eigenspace (7) into itself. The group  $D_4 \times Z_2$ , which is the symmetry of  $u_s$ , acts on this eigenspace.

Note that the action of  $D_4 \times Z_2$  on the critical eigenspace (7) has a nontrivial kernel generated by  $(x, y, u_1, u_2) \mapsto (1 - x, 1 - y, u_1, -u_2)$ . The factor group of the action modulo the kernel is isomorphic to  $D_4$ . Hence, the bifurcation of the saddle solution is a stationary bifurcation with  $D_4$  symmetry. This bifurcation is well-studied. (See, for example Golubitsky, Stewart & Schaeffer [1988], Chapter XVII, §4, 6.)

On the other hand, the action of  $D_4 \times D_4$  on the critical eigenspace (8) is faithful. The first bifurcation of the maximum solution is a stationary bifurcation with  $D_4 \times D_3$  symmetry, which has not (to the best of our knowledge) been studied before .

The EBL states that each one-dimensional fixed-point subspace of the group action contains a small-amplitude solution. A fixed point subspace of the action of a group  $G$  on  $\mathbf{R}^n$  is a subspace of  $\mathbf{R}^n$  which is pointwise invariant under the action of an isotropy subgroup  $\Sigma \leq G$ . See [Golubitsky, Stewart & Schaeffer, 1988] for more details. Table 2 describes the one-dimensional fixed point subspaces, and gives generators of the associated isotropy subgroups. Only one member of each group orbit of fixed-point subspaces is shown. For example, the subspace  $(r, 0)$  in the first row of Table 2 is in the same group orbit as the subspace  $(0, r)$ . For each of these subspaces, there is a group element (not in  $\Sigma$ ) which maps  $r \mapsto -r$ . Therefore, there is a pitchfork bifurcation in each of the fixed point subspaces. That is, the amplitude  $r$  satisfies  $r^2 \approx (\epsilon - \epsilon^*)/\alpha$  when  $r$  is small. Our analysis does not check all of the hypotheses needed to prove the existence of the pitchfork bifurcation. In particular, we do not compute  $\alpha$  so we cannot check that  $\alpha \neq 0$ . A rigorous computation could be done following the methods of [Allgower, Böhmer, & Zhen, 1994], Section 3.

Name	Fixed-Point Subspace	Generators of $\Sigma$ . $(x, y, u_1, u_2) \mapsto$
10	$(r, 0)$	$(1-x, y, u_1, -u_2)$ $(x, 1-y, u_1, u_2)$
11	$(r, r)$	$(y, x, u_1, u_2)$ $(1-y, 1-x, u_1, -u_2)$
1001	$(r, 0, 0, r)$	$(x, 1-y, u_1, -u_2)$
111-1	$(r, r, r, -r)$	$(y, x, u_1, -u_2)$
0011	$(0, 0, r, r)$	$(y, x, u_1, u_2)$ $(1-x, 1-y, u_1, -u_2)$
0010	$(0, 0, r, 0)$	$(1-x, y, u_1, -u_2)$ $(x, 1-y, u_1, u_2)$
1100	$(r, r, 0, 0)$	$(x, y, u_1, -u_2)$ $(y, x, u_1, u_2)$
1000	$(r, 0, 0, 0)$	$(x, y, u_1, -u_2)$ $(x, 1-y, u_1, u_2)$

Table 2: The solutions which bifurcate from the saddle solution (top two rows) and from the maximum solution (bottom six rows) at the first bifurcation. The six group orbits which bifurcate from the maximum solution represent 96 distinct solutions. The names correspond to subspaces of the critical eigenspaces (7) and (8). These are one-dimensional fixed-point subspaces for the group action described in Table 1. The third column lists the generators of the isotropy subgroup of each fixed-point subspace. A solution is invariant under the action of its isotropy subgroup.

The stationary bifurcation with  $D_4 \times D_3$  symmetry has many similarities to the Hopf bifurcation with  $D_4$  symmetry studied by Swift [1988], whose normal form has  $D_4 \times S^1$  symmetry, where  $S^1$  is the circle. There are three group orbits (circles) of solutions in the Hopf bifurcation, and the cubic truncation of the normal form is enough to make these solutions nondegenerate within the space of vector fields with the  $D_4 \times S^1$  symmetry. The cubic truncation of our stationary bifurcation with  $D_4 \times D_3$  symmetry is essentially the same. However, the three circles of solutions in the cubic truncation are degenerate. Higher degree terms are needed to break the circle of solutions into isolated solutions. For example, the cubic truncation of the normal form has a circle of solutions which is separated into 12 solutions in the group orbit of 1001, and 12 solutions in the group orbit of 111-1, by terms of degree 11 in the normal form! We have computed the degree three truncation of the normal form, but not the higher degree terms. If we can finish this calculation the results will be presented elsewhere. This bifurcation is very interesting, but further study of it would be a diversion from the current paper. The skeletal information provided by the EBL is enough to guide our numerical investigation.

## 4 Numerical Results

We wrote a C++ program that does the GNGA to find solutions of (1). In implementing Step 3 of the algorithm, we call the LAPACK routine DGELS to solve for the search direction. The results presented here use  $\delta = 1$  in Step 4 of the algorithm, so this is the “true” Newton’s method. We always took the tolerance in Step 7 to be  $TOL \leq 10^{-13}$ . The number of modes was  $M \geq 242$ , with some exceptions that are clearly labelled in our results. The simplicity of the domain and eigenfunctions allowed us to do the numerical integrations exactly, except for roundoff error (see [Neuberger & Swift, 2001]). Newton’s method typically converged in 5 to 7 iterations. Each Newton step took about 3 seconds for  $M = 242$  up to about a minute

for  $M = 538$ , which was the largest  $M$  we used.

The predictions listed in Table 2 were used to guide the initial guess for nontrivial solutions near the bifurcations. Once a solution is found, the larger amplitude solutions on the same branch can be obtained by stepping  $\epsilon$  down, using the solution at the previous value of  $\epsilon$  as an initial guess. We followed all of the bifurcating branches down to  $\epsilon = 0.1$ . The resulting bifurcation diagram of  $J_\epsilon(u)$  versus  $\epsilon$  is shown in Figure 2.

The EBL gives only the crudest information about the bifurcations we studied. For example, it does not claim to list *all* solutions which bifurcate. Nevertheless, it appears from our numerical calculations that no solutions, other than those listed in Table 2, bifurcate from the saddle solution at  $\epsilon \approx 0.4399$  or from the maximum solution at  $\epsilon \approx 0.4502$ . The numerical results in Figure 2 start at  $\epsilon = 0.43$ . There are indications that the 1001 and 111-1 solutions each undergo two secondary bifurcations in the interval  $0.43 < \epsilon < 0.4502$ , but a report on this must await a more detailed exposition of the bifurcation with  $D_4 \times D_3$  symmetry.

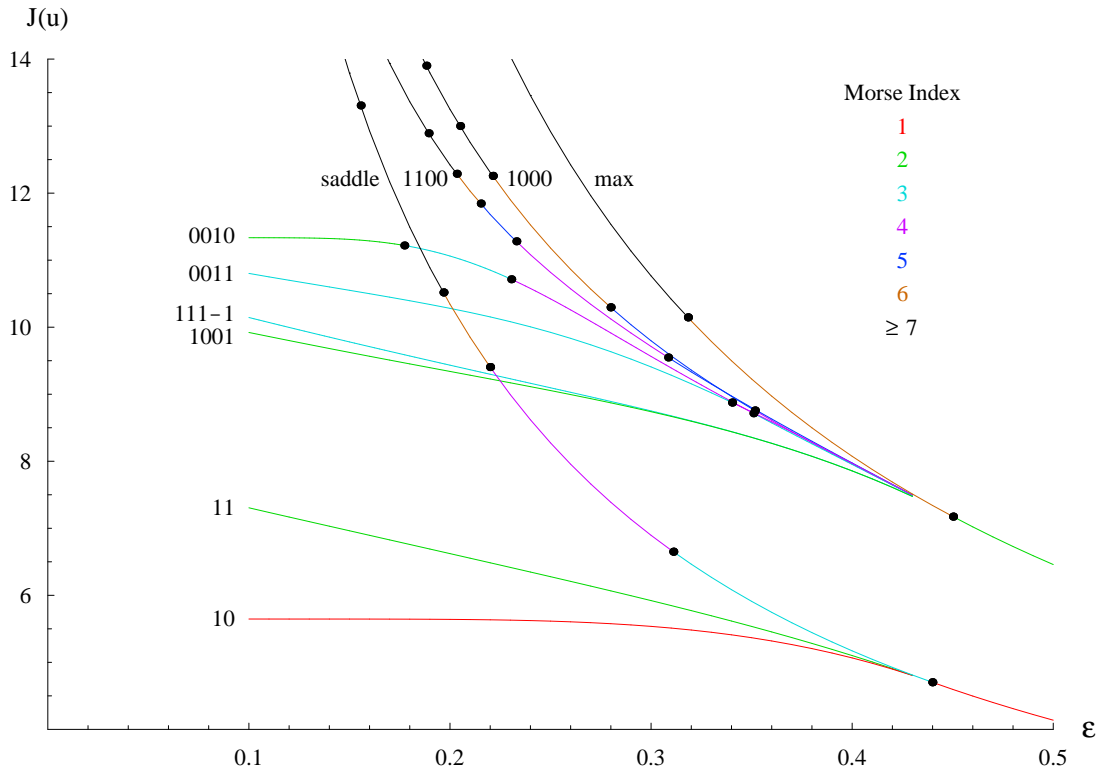


Figure 2: This bifurcation diagram shows the saddle solution, the maximum solution, and the solutions which bifurcate off these trivial solutions at the first bifurcation as  $\epsilon$  is decreased. The minimum solution, which is not shown, has  $J = 0$  and MI 0 for all  $\epsilon$ . The dots indicate a bifurcation point, where the MI changes.

The solutions we found numerically at  $\epsilon = 0.1$  are shown in Figure 3. As expected, many solutions appear to have  $u(x, y)$  very close to one of the three minima of the the potential  $W$  everywhere except along thin transition regions. These solutions have a finite value of  $J_\epsilon(u)$ , and  $W(u(x, y)) = 0$  almost everywhere in the limit  $\epsilon \rightarrow 0$ .

In contrast,  $\lim_{\epsilon \rightarrow 0} J_\epsilon(u)$  does not exist for the 1000 solution and the 1100 solution. These solutions lie in the invariant subspace where  $u_2 \equiv 0$ . The system (1) reduces to a scalar PDE for  $u_1(x, y)$  with a *nonsymmetric* double well potential. The saddle point in the triple well potential becomes the higher local minimum in the double well potential. As  $\epsilon$  decreases, the region where  $u \approx u_s$  grows to cover most of the

square.

The 10 solution is the MI 1 mountain pass solution used by Flores, Padilla & Tonegawa [2001] to prove the existence of a MI 2 solution. The properties of the MI 2 solution are not supplied by the proof, but the authors conjecture that the MI 2 has a triple junction where three interfaces meet at  $120^\circ$  angles. The 1001 solution has both MI 2 and a triple junction, so this is presumably the solution implied by the theorem of Flores, Padilla & Tonegawa [2001]. For the square region, there is another triple junction solution, with higher energy and MI 3: the 111-1 solution.

Figure 4 shows the apparent limit, as  $\epsilon \rightarrow 0$ , of the solutions which have finite  $J_\epsilon$  in that limit. The interface has minimal energy when it has no curvature. If the boundary of  $\Omega$  is smooth, the interface is perpendicular to the boundary. If we rounded off the corners of the square, then the interface could touch anywhere in the arc. Therefore we assume that the interfaces are line segments which can touch a corner of the square in the limit  $\epsilon \rightarrow 0$ . The limiting patterns of the 0011 solution and the 0010 solution are not obvious. We looked at animations of the pattern with  $\epsilon$  changing in time, which can be found at the website [http://math.nau.edu/~jws/nrs\\_paper/](http://math.nau.edu/~jws/nrs_paper/). The animations clearly show the two triple junctions of the 0011 solution coming together to form the quadruple junction shown in Figure 4. The red strip in the middle of the 0010 solution narrows as  $\epsilon$  decreases. We conjecture that the width is asymptotically proportional to  $\epsilon$ , so that the pointwise limit of the solution is red on a line segment.

Figures 5 and 6 show why we stopped our bifurcation branches at  $\epsilon = 0.1$ , for which  $\epsilon^2$  is quite small. Figure 5 shows the bifurcation curves obtained for 6 different choices of the cutoff parameter  $k$ . Recall that we included all modes  $\psi_{m,n}$  for which  $\lambda_{m,n} = \pi^2(m^2 + n^2) < k^2$ . Thus a choice of  $k$  yields  $\widetilde{M}$  modes for  $u_1$ , and the same number for  $u_2$ , giving  $M = 2\widetilde{M}$  modes in all. When  $\epsilon$  gets small, the solution approaches a step function, and our Fourier mode approximation exhibits the Gibbs phenomenon. The deviation of  $u$  from a minimum of  $W$  causes a large value of  $J$ , as seen in Figure 5. Furthermore, the solutions tend to “jump” off the branch when  $\epsilon$  gets close to 0.1. It would be easy to implement an algorithm where the solution at the new  $\epsilon$  value was predicted by a linear approximation. This would help the problem of “branch jumping,” but the Gibbs phenomenon would still be there. We did not add this feature to our C++ code.

We presume that the solution found by the GNGA converges to a solution of the PDE as the number of modes in the Galerkin space  $G$  increases without bound. While we have no proof of a convergence result, we are convinced that our results are not spurious due in part to a computation of the  $L^2$  error of the PDE:

$$\text{error} = \sqrt{\int_{\Omega} |-\epsilon^2 \Delta u + \nabla W(u)|^2 dx dy}.$$

Some results of this error calculation are shown in Figure 6. As expected, the error decreases as the number of modes increases. On this log-linear plot the points fall on approximate straight lines, which suggests that

$$\text{error} \propto \text{Exp}(-\sqrt{\lambda_{\max}})$$

where the Galerkin space is  $G = \{\psi_i : \lambda_i < \lambda_{\max}\}$ . We have observed this same rule of error decay in ODEs ( $\Omega \subset \mathbf{R}$ ). It would be interesting to see if this trend extends to spatial domains ( $\Omega \subset \mathbf{R}^3$ ).

Figure 5 also shows how we estimate  $J_0 := \lim_{\epsilon \rightarrow 0} J_\epsilon(u)$ . We made a linear fit of  $J_\epsilon$  versus  $\epsilon$  using the data in the interval  $0.1 \leq \epsilon \leq 0.13$  for all of the solutions listed in Table 3. The third column shows the total length of the interface for the conjectured limiting solution shown in Figure 4. Most of the lengths are trivial to compute, with the exception of the 111-1 solution whose interface has length  $(\sqrt{2} - \sqrt{3} + 2\sqrt{2})/\sqrt{3} \approx 1.932$ . This length can be computed using the law of sines on the  $15^\circ$ - $45^\circ$ - $120^\circ$  triangles which make up the blue and green regions, where  $\sin(15^\circ)$  is obtained from a half-angle formula.

The most striking feature of Table 3 is that  $J_0$  is approximately proportional to the length of the interface. Indeed, a theorem of Baldo (see [Baldo, 1990] and Theorem 1.1 of [Sternberg & Zeimer, 1994]) states that  $J_0$  is proportional to the  $H^1$  measure (length) of the interface.

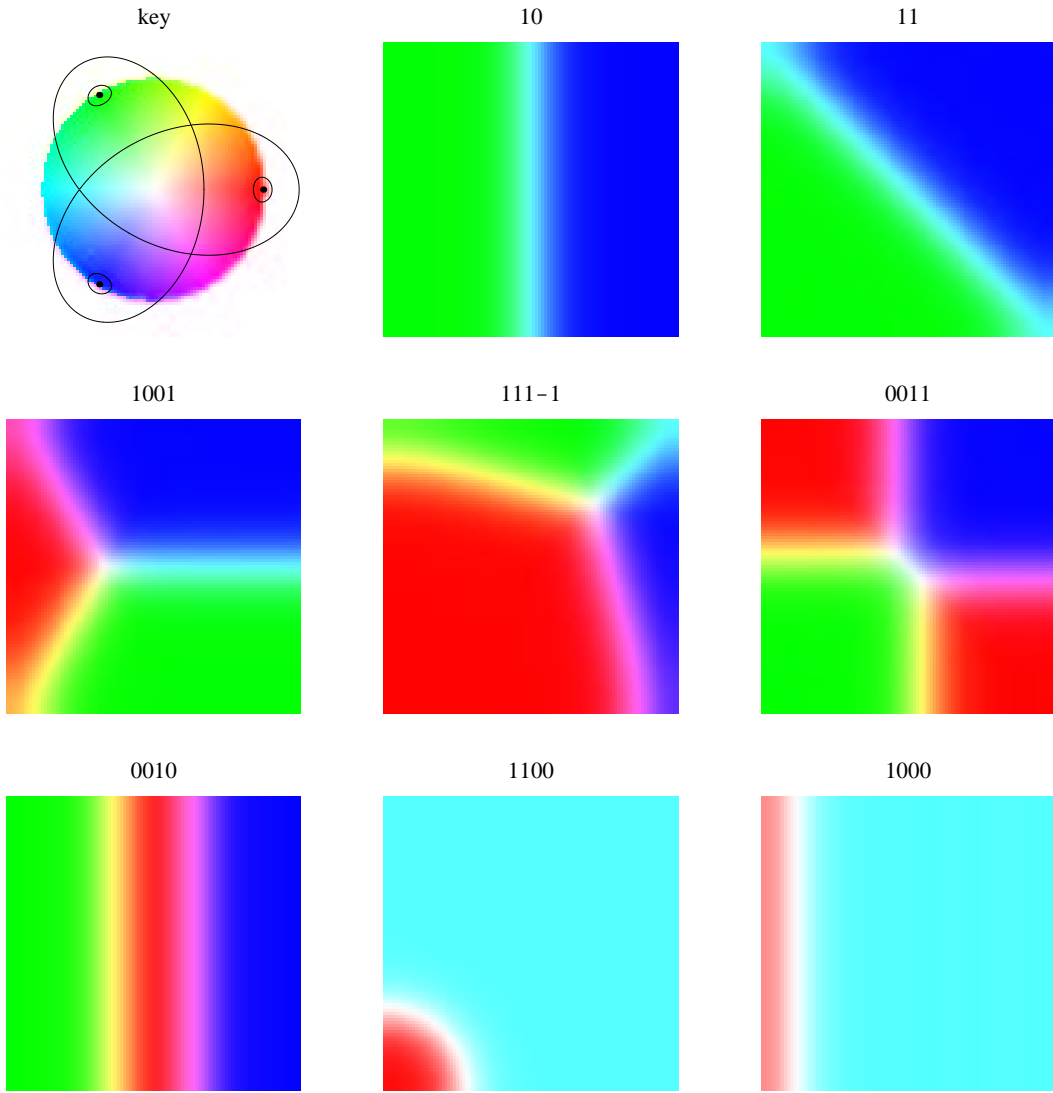


Figure 3: The solutions listed in Table 2. All of these solutions are computed at  $\epsilon = 0.1$ , where the nonlinear corrections to the critical eigenspace are significant. The key at the upper left shows a few contours of the potential  $W$  to indicate how the color codes the value of  $u(x,y)$ . These large amplitude solutions have the same symmetry they did at the bifurcation, as listed in Table 2.

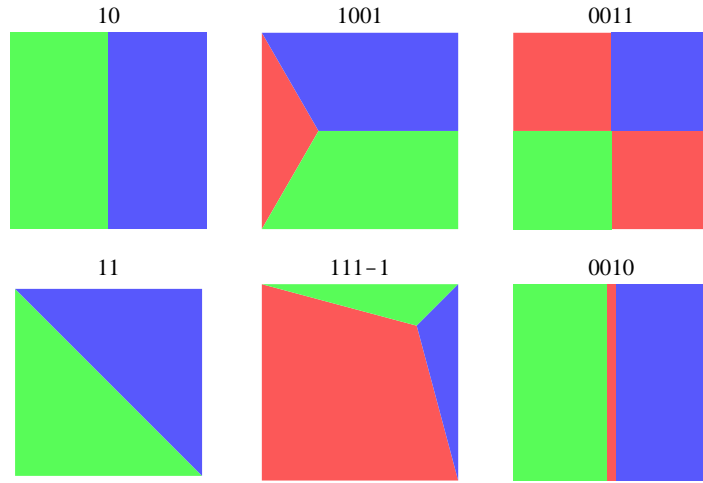


Figure 4: Our conjectures for the limiting solutions as  $\epsilon \rightarrow 0$ . We are guided by animations of the solutions as a function of  $\epsilon$ .

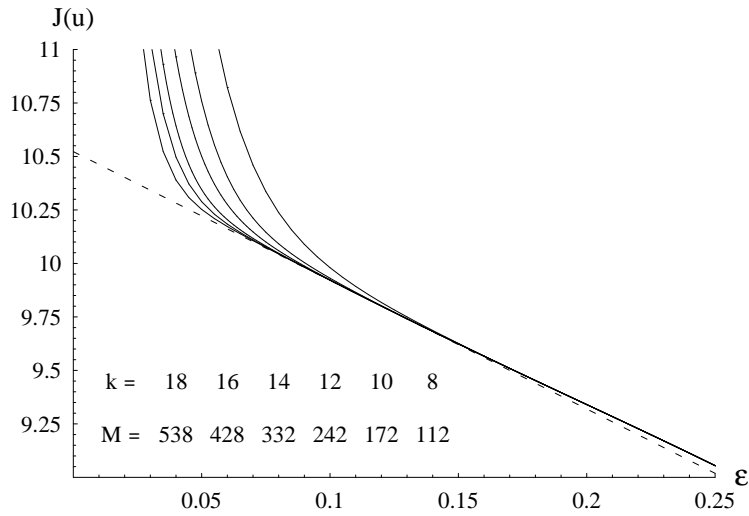


Figure 5: Six different curves of  $J$  versus  $\epsilon$  for the 1001 solution are shown, each with a different number of modes in the GNGA. The dotted line is an extrapolation of the linear fit of the most accurate curve (with  $k = 18$  giving  $M = 538$  modes) in the interval  $0.1 \leq \epsilon \leq 0.13$ . The results suggest that  $\lim_{\epsilon \rightarrow 0} J(u) \approx 10.5$  for the 1001 solution.

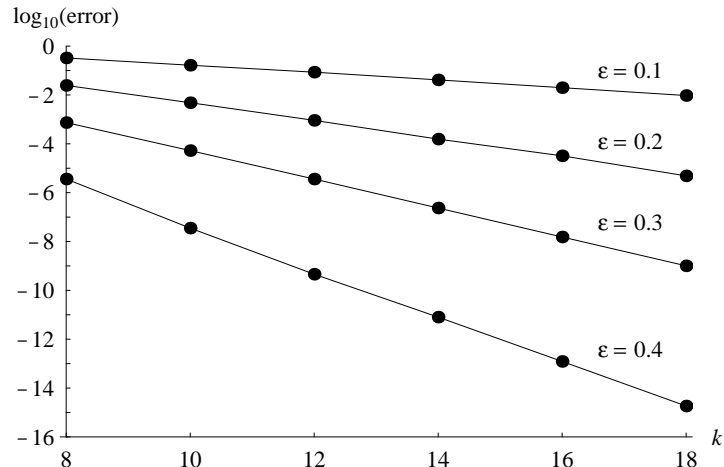


Figure 6: The  $L^2$  error of the PDE, as a function of the cutoff parameter  $k$ , for the 1001 solution at four different values of  $\epsilon$ . The lines are to guide the eye. As expected the larger amplitude solutions, with smaller  $\epsilon$ , have more error. The error at  $\epsilon = 0.1$ , with  $k = 18$ , is  $9.50 \times 10^{-3}$ .

Solution	estimate of $J_0$	Length $L$	$J_0/L$
10	5.65	1	5.65
11	7.99	$\sqrt{2}$	5.65
1001	10.52	$1 + \sqrt{3}/2$	5.64
111-1	10.88	1.932...	5.63
0011	11.31	2	5.65
0010	11.35	2	5.68

Table 3: The limiting energy  $J_0$  is computed by the method demonstrated in Figure 5. The total length of the interface  $L$  is computed geometrically for the solutions shown in Figure 4.

## 5 Conclusion

Since concluding this research project, we have begun investigating several extensions. For example, one may wish to pursue the effect of having a nonsymmetric region  $\Omega$  or a nonsymmetric triple-well potential. We have already developed and tested algorithms for computing a basis of eigenfunctions of the Laplacian for general regions. Implementing our method on non-square or nonsymmetric regions is not difficult, and the properties of the resulting pattern formations may be interesting and useful. We have already obtained good approximations to the triple-junction solution when the region  $\Omega$  is a disk in  $\mathbf{R}^2$ . Further investigation could be done by following bifurcation branches from the other bifurcation points, where other pattern formations could be observed.

By modifying our basis and functional slightly, we were able to code and test the related Ginzburg-Landau problem

$$\begin{aligned} -\epsilon^2 \Delta u - u(1 - |u|^2) &= 0 \text{ in } \Omega, \\ u &= g \text{ on } \partial\Omega, \end{aligned} \tag{9}$$

where  $u$  is a complex valued function and  $g : \partial\Omega \rightarrow \mathbf{C}$ . Using appropriate choices for the boundary function  $g$ , we are able to model vortices (see [Almeida & Bethuel, 1998] and [Bethuel, Brezis & Hélein, 1994]).

A next possible step is to adapt our algorithm to study the so-called “full Ginzburg-Landau” system. In

[Neuberger, 1997] the functional for this substantially more difficult problem is given:

$$E(u, A) = \int_{\Omega} \left( \frac{1}{2} |(\nabla - iA)u|^2 + \frac{1}{2} |\nabla \times A - H_0|^2 + \frac{\kappa^2}{4} ((1 - |u|^2)^2) \right) dx, \quad (10)$$

The region  $\Omega$  is a subset of  $\mathbf{R}^p$ , for  $p = 2$  or  $p = 3$ . Here the unknowns are the order parameter  $u \in H^{1,2}(\Omega, \mathbf{C})$  and the vector potential  $A \in H^{1,2}(\Omega, \mathbf{R}^p)$ . If the applied magnetic field  $H_0$  is identically zero, then we can assume that  $A(x) = 0$  and the Euler-Lagrange equation of (10) reduces to (9), where  $\kappa = 1/\epsilon$ . One challenge that presents itself in investigating this problem is in dealing with the natural boundary conditions

$$(\nabla \times A) \times \eta = H_0 \times \eta \text{ and } ((\nabla - iA)u) \cdot \eta = 0,$$

where  $\eta$  is as before the outward unit normal.

There is a great body of literature considering various facets of the analysis of Ginzburg-Landau problems, of which we have referenced only a few select works. References to numerical investigations of these problems are somewhat sparse. Very little can be found concerning analysis or numerics in the “full Ginzburg-Landau” case.

Our method works very well, even for fairly small  $\epsilon$ . We are able to make qualitative and quantitative conjecture about the  $\epsilon \rightarrow 0$  limit with the GNGA. Extremely small values of  $\epsilon$  yield solutions that are close to step-functions, where a basis of cosine or sine functions has some limitations. Features such as vortices cause similar problems. One could consider using an alternate choice of basis for  $L^2 \times L^2$  and  $H \times H$ . In fact, at the time of this writing the use of a basis of wavelets is being investigated. We wish to emphasize, however, that the eigenfunction basis is in many ways the natural choice and has yielded satisfactory results for reasonably small values of  $\epsilon$ .

## Acknowledgements

We wish to thank Prof. P. Padilla of UNAM for many helpful discussions. This work was partially supported by NSF grant DMS-0074326.

## References

- Adams, R. A. [1975] *Sobolev Spaces*, (Academic Press: New York).
- Allgower, E., Böhmner, K. & Zhen, M. [1994], “Branch switching at a corank-4 bifurcation point of semi-linear elliptic problems with symmetry,” *IMA J. Numer. Anal.*, **14** (2), 161–182.
- Allgower, E. & Georg, K. [1990], *Numerical continuation methods. An introduction*. Springer Series in Computational Mathematics, **13**, (Springer-Verlag).
- Almeida, L. & Bethuel, F. [1998] “Topological Methods for the Ginzburg-Landau Equations,” *J. Math. Pures Appl.* **77**, 1-49.
- Baldo, S. [1990] “Minimal Interface Criterion for Phase Transitions in Mixtures of Cahn-Hilliard Fluids,” *Ann. Inst. H. Poincaré Anal. Non Linéaire* **7**, 37–65.
- Bank, R. & Mittelmann, H. [1989], “Stepsize selection in continuation procedures and damped Newton’s method. Continuation techniques and bifurcation problems,” *J. Comput. Appl. Math.* **26** (1-2), 67–77.
- Bethuel, F., Brezis, H. & Hélein, F. [1994] *Ginzburg-Landau Vortices* (Birkhauser, Boston).
- Flores, G., Padilla, P. & Tonegawa, Y. [2001] “Higher Energy Solutions in the Theory of Phase Transitions: A Variational Approach,” *J. Differential Equations* **169**(1), 190–207.

- Gilbarg, D & Trudinger, N. [1983] *Elliptic Partial Differential Equations of Second Order* (Springer-Verlag, Berlin, New York). Golubitsky, M., Stewart, I. & Schaeffer, D.G. [1988] *Singularities and Groups in Bifurcation Theory, Volume II*, Applied Mathematical Sciences **69**, (Springer-Verlag).
- Milnor, J. [1963] *Morse Theory* (Princeton University Press, Princeton ). Neuberger, J. M. & Swift, J. W. [2001] “Newton’s Method and Morse Index for Semilinear Elliptic PDEs,” *Int. J. Bifurcation and Chaos* **11**(3), 801–820.
- Neuberger, J. W. [1997] *Sobolev Gradients and Differential Equations*, Lecture Notes in Mathematics **1670**, (Springer-Verlag, Berlin).
- Sattinger, D. H. [1979] *Group Theoretic Methods in Bifurcation Theory*, Lecture Notes in Mathematics **762**, (Springer-Verlag, Berlin, Heidelberg, New York).
- Sternberg, P. & Zeimer, W. P. [1994] “Local Minimizers of a Three-Phase Partition Problem with Triple Junctions,” *Proc. Roy. Soc. Edinburgh* **124**(A), 1059–1073.
- Swift, J. W. [1988], “Hopf bifurcation with the symmetry of the square,” *Nonlinearity* **1**, 333–377.
- Vanderbauwhede, A. [1982] *Local Bifurcation and Symmetry*, Res. Notes in Math. **75**, Pitman, Boston).
- Zhen, M. [2000], *Numerical Bifurcation Analysis for Reaction Diffusion Equations*, Springer Series in Computational Mathematics, **28**, (Springer-Verlag).